Supplementary Online Material for

Carbon isotopes and Pa/Th response to forced circulation changes: a model perspective

L. Missiaen[1,2], N. Bouttes[1], D.M. Roche[1,3], J-C. Dutay[1], A. Quiquet[1,4], C. Waelbroeck[1], S. Pichat[5,6], J-Y Peterschmidtt[1]

[1]Laboratoire des Sciences du Climat et de l'Environnement, LSCE/IPSL, CEA-CNRS-UVSQ-Université Paris-Saclay, F-91198 Gif-sur-Yvette, France.
[2]Climate Change Research Centre, University of New South Wales, Sydney, Australia
[3]Vrije Universiteit Amsterdam, Faculty of Science, Cluster Earth and Climate, de Boelelaan 1085, 1081HV Amsterdam, The Netherlands
[4]Institut Louis Bachelier, Chair Energy and Prosperity, Paris, 75002, France
[5]Université de Lyon, ENS de Lyon, Laboratoire de Géologie de Lyon (LGL-TPE), F-69007 Lyon, France.
[6]Climate Geochemistry Department, Max Planck Institute for Chemistry, Mainz, Germany.

Correspondence to: Lise Missiaen (l.missiaen@unsw.edu.au)

The supplementary material includes:

- **Supplementary text**

Text S1: Model Tuning
Text S2: Dissolved and particulate ^{231}Pa and ^{230}Th

- **Supplementary figures**

Fig. S1. Zonally averaged dissolved and particulate ^{231}Pa, ^{230}Th and Pa/Th on the N-S Atlantic section.
Fig S2. Model-data comparison of dissolved and particulate Pa, Th and Pa/Th along the GEOTRACES transect GA03
Fig S3. Model-data comparison of dissolved Pa, Th and Pa/Th along the GEOTRACES transect GA02S
Fig. S4. Atlantic meridional stream function
Fig. S5. Proxy anomalies in the eastern Atlantic basin
Fig. S6. Proxy response times in the eastern Atlantic basin
Fig. S7. Selected time series during the hosing experiments.
Fig S8. Evolution of the and phosphate anomalies on the Atlantic N-S section

- **Supplementary tables (in a separate xlsx file)**

Tab. S1. Compilation of Kd and fractionations factors from observations and model studies
Tab. S2. Latin Hypercube Sampling inputs and best fit parameters

Text S1: Model Tuning

We chose to represent the non-equilibrium relation between dissolved and particulate Pa and Th. Therefore, for both isotopes, we considered adsorption and desorption coefficients (K_{adsorp} and K_{desorp}) and transported both dissolved and particulate activities instead of transporting a total activity that is split into particulate and dissolved activities using partition coefficients (K_d-describing equilibrium situation). If some observations are available to constrain the K_d coefficients (*e.g.* (Chase et al., 2002; Hayes et al., 2015b)), a wide range of K_d values have been observed in the modern ocean and to date, no consensus value is available. Concerning adsorption and desorption coefficients, even less constraints are available. Equation 4 only allows to determine a range for K_{adsorp}/K_{desorp} ratio from the available ranges of K_d coefficients. As a first approach, we chose here to consider a single and constant K_{desorp} value but there is no theoretical reason to prevent K_{desorp} to be different for POC, $CaCO_3$ or opal particles. Thus, there are six $\sigma_{i,j}$ and potentially six K_{desorp} coefficients to adjust with the available observational data (that are ranges for the six K_d and three F(Th/Pa) values).

In this study we chose to tune the three Th σ coefficients and the three F(Th/Pa) fractionation factors. We used a LHS methodology to produce 60 sets of final $\sigma_{i,j}$ coefficients to be tested. Because there are wide ranges of possible Th σ coefficients and F(Th/Pa), it is possible that the LHS probably did not capture the right balance between the scavenging efficiency of the different particle types. Indeed, in the majority of the tested parameters sets, the $K_{d-Pa,opal}$ was greater than $K_{d-Pa-CaCO3}$ or $K_{d-Pa-POC}$. In other words, in most of our tuning tests, opal was the main scavenger for Pa. This could explain why in our model we obtain low dissolved Pa concentrations in the opal belt area compared to the observations (Figure S1). Indeed, as for Pa the highest K_d is attributed to opal, Pa is mainly retrieved from the water column and exported towards the sediments via the opal sedimentary flux throughout the global ocean. Thus, in that configuration, tests to reduce the $\sigma_{Pa,opal}$ lead to a general increase of the dissolved Pa in the water column. This deterioration of the general model-data agreement is likely a consequence of reduced Pa scavenging in the high latitude and advection of the signal elsewhere.

Additionally, the model-data agreement evaluation was problematic: when calculating the Root Mean Squared Error (RMSE) for the four tracers (4 metrics corresponding to: dissolved Pa, dissolved Th, particulate Pa and particulate Th) between the observations compiled in (Dutay et al., 2009) and references therein and the closest model grid-cell, we observed that the best simulations for Pa did not correspond to the best simulations for Th and

vice versa. When trying to combine the best $\sigma_{i,j}$ parameters for Pa and their counterparts for Th from 2 distinct simulations, we observed that the F(Th/Pa) were out of the observation range. To choose the best fit simulation we established a classification of the 60 tuning simulations based on the RMSE between model output and the observation for each of our five metrics (particulate Pa, particulate Th, dissolved Pa and dissolved Th and sedimentary Pa/Th). The best fit simulation was selected among the candidates that appeared in the 30 first ranks for each metric after visual evaluation of the model-data agreement (using tools such as Figures 1 S1 to S3).

One way to overcome the tuning issues highlighted above could be to select the six $\sigma_{i,j}$ coefficients as input parameters of the LHS, generate a significantly higher number of parameter sets and discard a posteriori the parameters set which do not fulfill the observational F(Th/Pa) constraints. This would also allow to ensure testing configurations in which opal is not the main scavenger for Pa.

Text S2: Dissolved and particulate ^{231}Pa and ^{230}Th

Figure S1-S3 show the climatological annual mean simulated dissolved and particulate ^{231}Pa and ^{230}Th activities in the water column for the last 100 years of the equilibrium best fit-simulation on a zonally averaged Atlantic N-S section as well as on GEOTRACES transects GA02S and GA03. Overall, we succeed in producing a realistic range for both dissolved and particulate ^{231}Pa and ^{230}Th concentrations. These concentrations generally increase with depth, which is expected in the reversible scavenging theoretical model and consistent with observations. The comparison with observations along the GEOTRACES transects reveals that the model produces some major characteristics of the tracers distributions in the deep ocean. In particular the observed East-West gradients associated with NADW in the ^{230}Th and ^{231}Pa dissolved distributions along the GA03 section are simulated. The results along the GA02S section are more complicated to evaluate because the tracers distributions are not only controlled by NADW southward propagation, but also by significant lithogenic scavenging from nepheloid layers and atmospheric dust deposition (Deng et al., 2014). Nevertheless the model produces the main characteristics observed along the GA02S section, especially the North-South gradients in ^{230}Th and ^{231}Pa/^{230}Th distributions, even if the concentration of ^{231}Pa in the southern ocean are too low compared to observations, similarly to the results of the NEMO/PISCES model (van Hulten et al., 2018).

However, our model generally simulates lower particulate and dissolved concentrations than what is measured in the present-day ocean (Figure S1-S3), in particular at the surface.

Model to data agreement is generally better at depths > 2,500 m than closer to the surface, which, together with the too low dissolved concentrations, indicate that our scheme tends to scavenge too fast. In other words, Pa and Th quickly adsorb on the settling particles and are too rapidly removed from the water column. The fast scavenging regime of our model is also consistent with the Kd coefficients obtained for our PI best-fit iLOVECLIM simulation that are in the upper range of the observations (Table 2- Table S1) and are significantly higher than the ones reported in (van Hulten et al., 2018). As evidenced by (Dutay et al., 2009), the scavenging intensity and efficiency strongly depends on the particles concentration and settling speed (Eq 4). In this study we applied the particles concentrations from PISCES but used different settling speed. Indeed, we considered only one particle size with a settling speed of 1,000 m/y, which is close to the settling speed of the small particles considered in (van Hulten et al., 2018) (2m/d ~730 m/y) but much lower than that considered for big particles (50 m/d ~18250 m/y). Using the $_{231}$Pa and $_{230}$Th content of suspended particles and water samples, (Gdaniec et al., 2018) evaluated the particle settling speed between 500 and 1,000 m/y which is close to the value used in our model simulations. Including the settling speed into the tuning coefficients could be part of further developments to increase model-data agreement under PI conditions.

Finally, our model set-up does not currently account for Pa and Th scavenging by lithogenic particles. Reanalysis of observational data (e.g.(Luo and Ku, 2004)) evidenced the important role of the lithogenic particles in the Pa and Th scavenging. In some model studies, lithogenic particles have been found unimportant (e.g. (Siddall et al., 2005)), whereas in other model studies lithogenic particles carry most of the particle bound Pa and Th (e.g. (van Hulten et al., 2018))The importance of the lithogenic particles is thus model dependent and probably strongly relies on the adsorption coefficient tuning, the problem being largely underconstrained. A better model-data agreement could also be achieved by including lithogenic particles in the model.
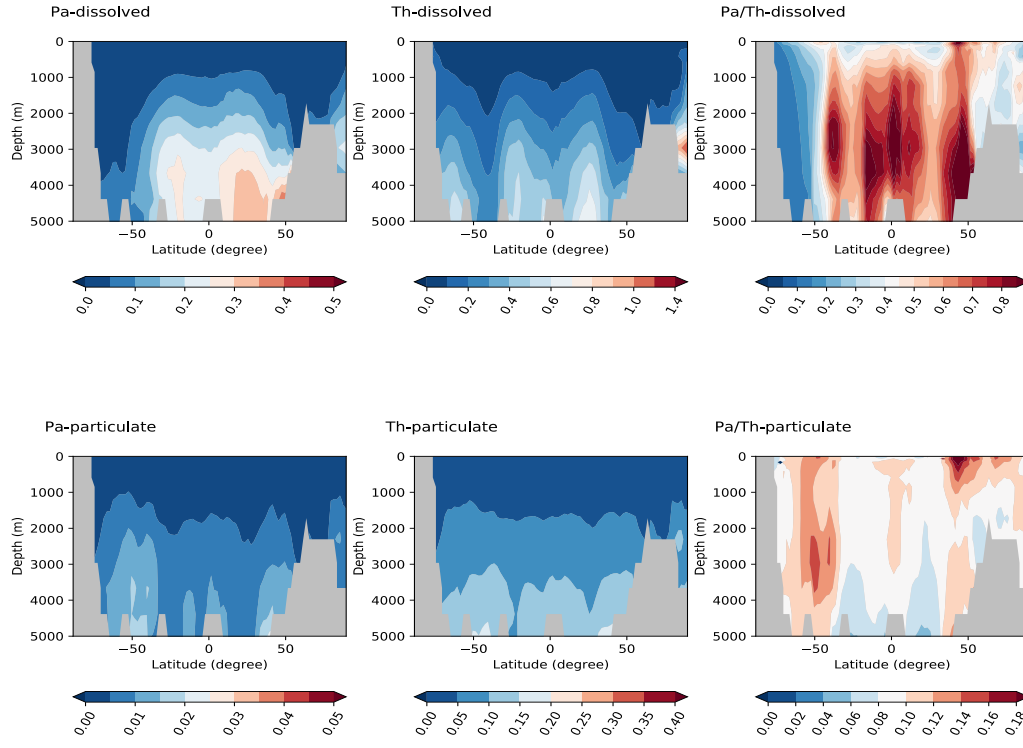
Figure S1: Zonally averaged dissolved (top) and particulate (bottom) Pa activity (left), Th activity (center) and Pa/Th ratio (right) simulated by iLOVECLIM on the N-S Atlantic section. Pa and Th activities are given in dpm.m-3, the Pa/Th ratios are dimensionless.
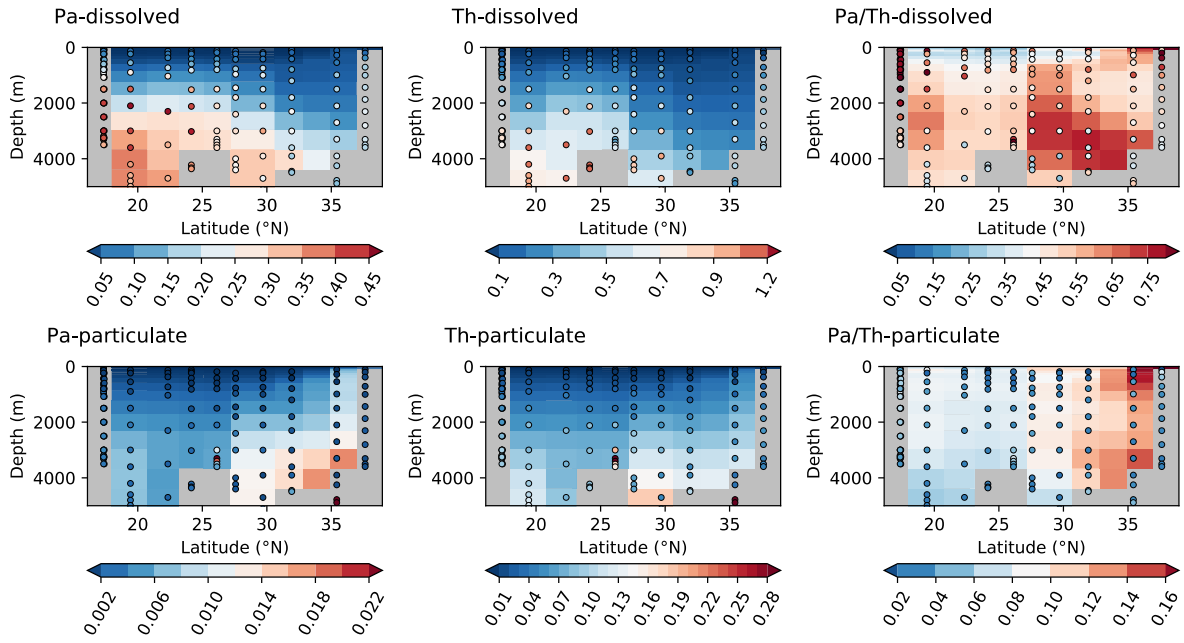
Figure S2: Simulated (background color) dissolved (top) and particulate (bottom) Pa activities (left), Th activities (center) and Pa/Th ratios (right) along the GEOTRACES transect GA03. The color dots represent the observed dissolved and particulate Pa and Th activities corrected for any ^{231}Pa and ^{230}Th source other than the water column U-decay (excess fractions) as compiled in (Hayes et al., 2015a, 2015b). The transect strictly represents the closest model water column relative to the GA03 GEOTRACES stations. The Pa and Th activities are given in dpm.m$_3$.
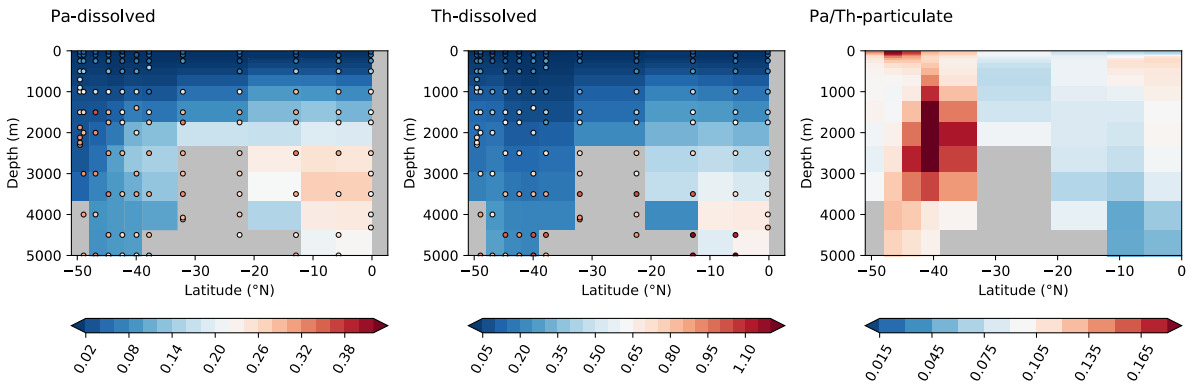

Figure S3: Simulated (background color) dissolved Pa activities (left), Th activities (center) and Pa/Th ratios (right) along the GEOTRACES transect GA02S. The colors dots represent the observed dissolved Pa and Th activities corrected for any ^{231}Pa and ^{230}Th source other than the water column U-decay (excess fractions) as compiled in (Deng et al., 2014). The transect strictly represents the closest model water column relative to the GA02S GEOTRACES stations. The Pa and Th activities are given in dpm.m$_3$.
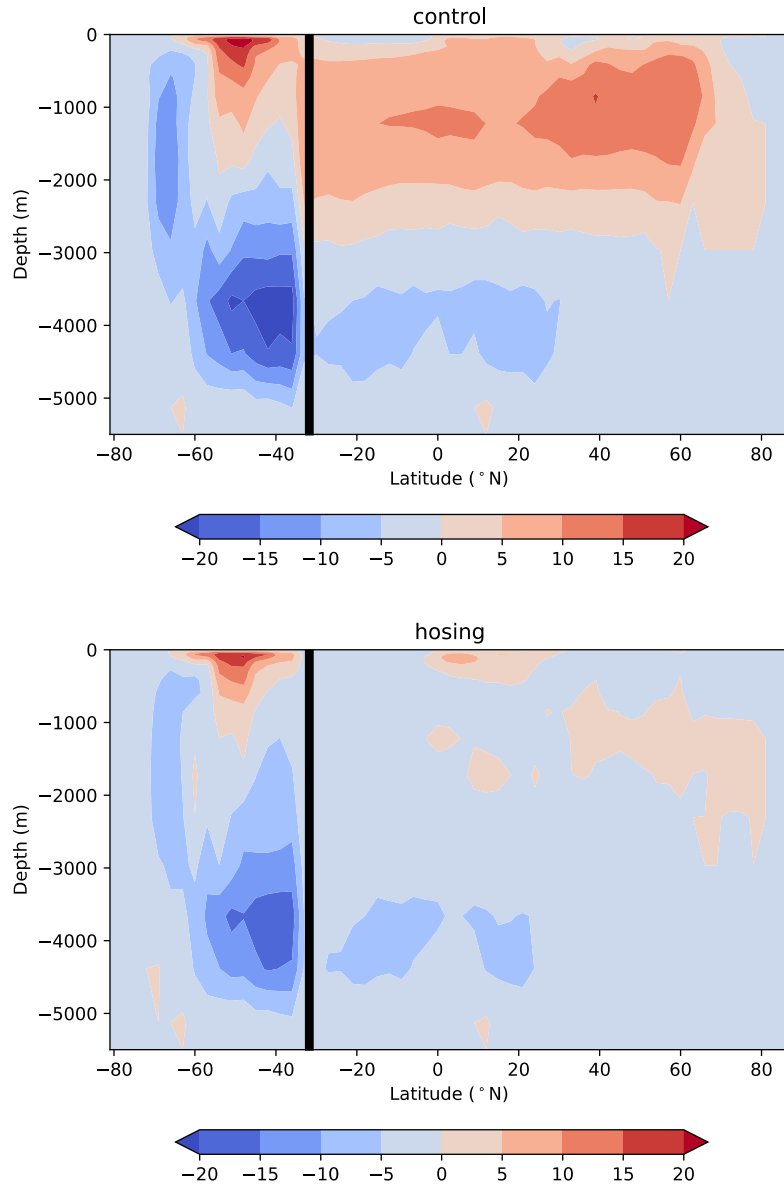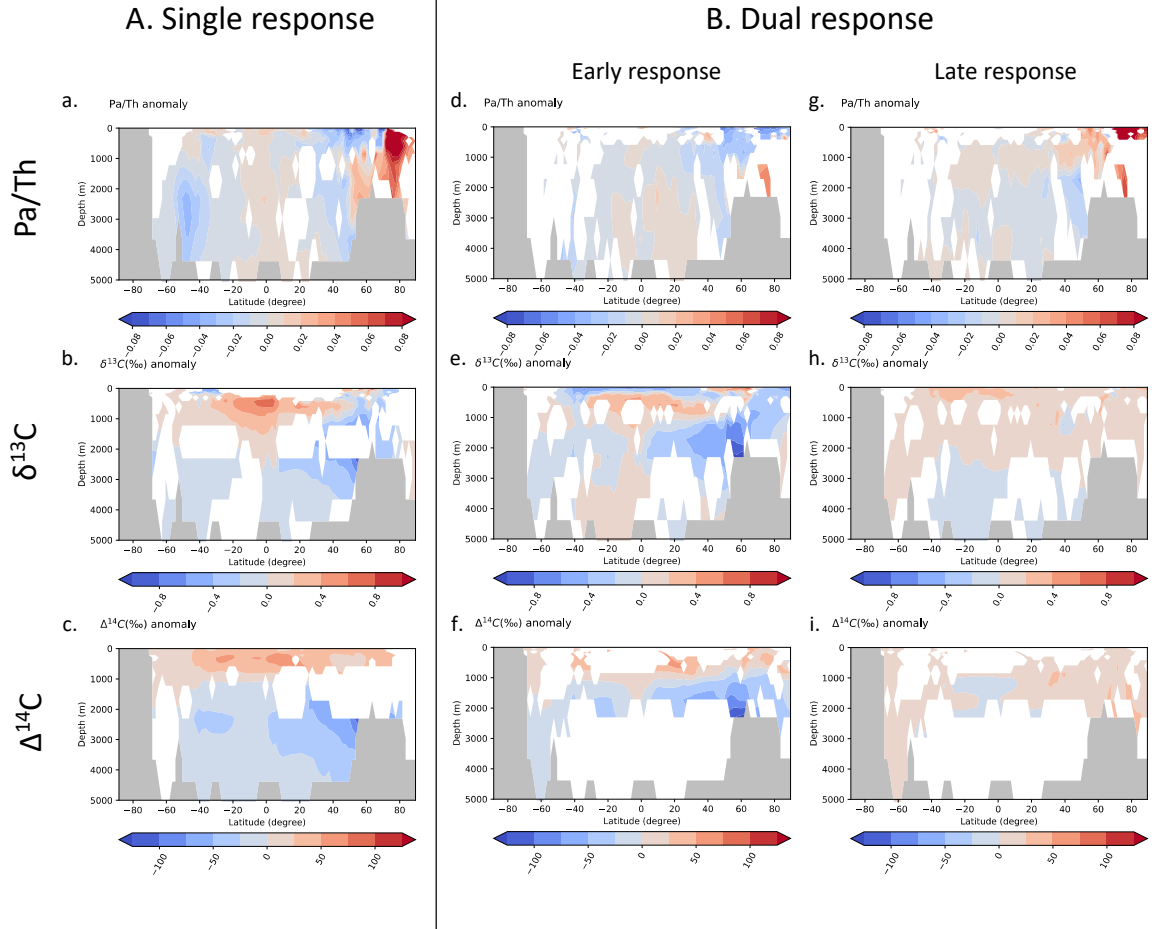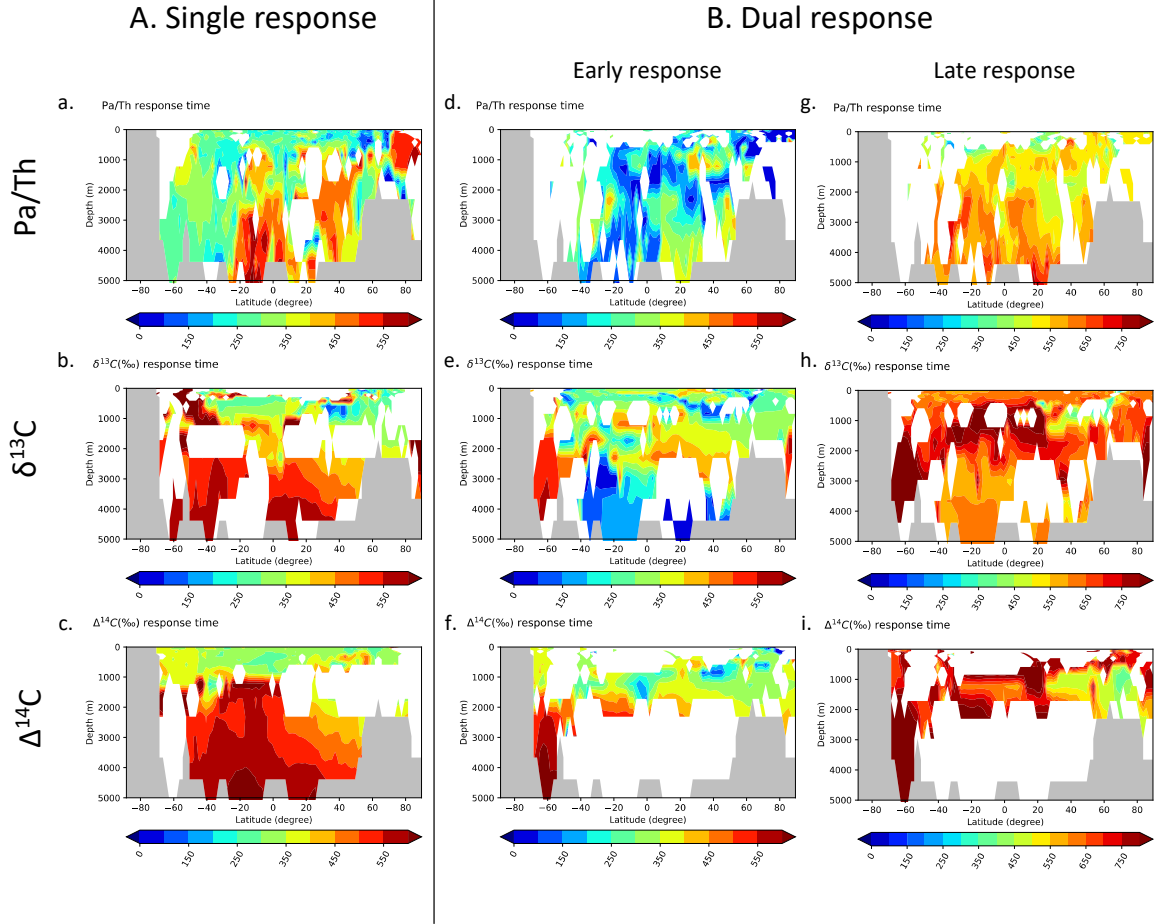
Figure S4: Atlantic meridional stream function (Sv)
The upper panel shows the average stream function during the control period of simulation (i.e. the first 300 years under PI conditions). The lower panel presents the average stream function during the last 100 years of freshwater forcing (year 500 to y 600). The vertical
black line indicates the limit between the Southern Ocean south of 32°S and the Atlantic Ocean north of 32° S.
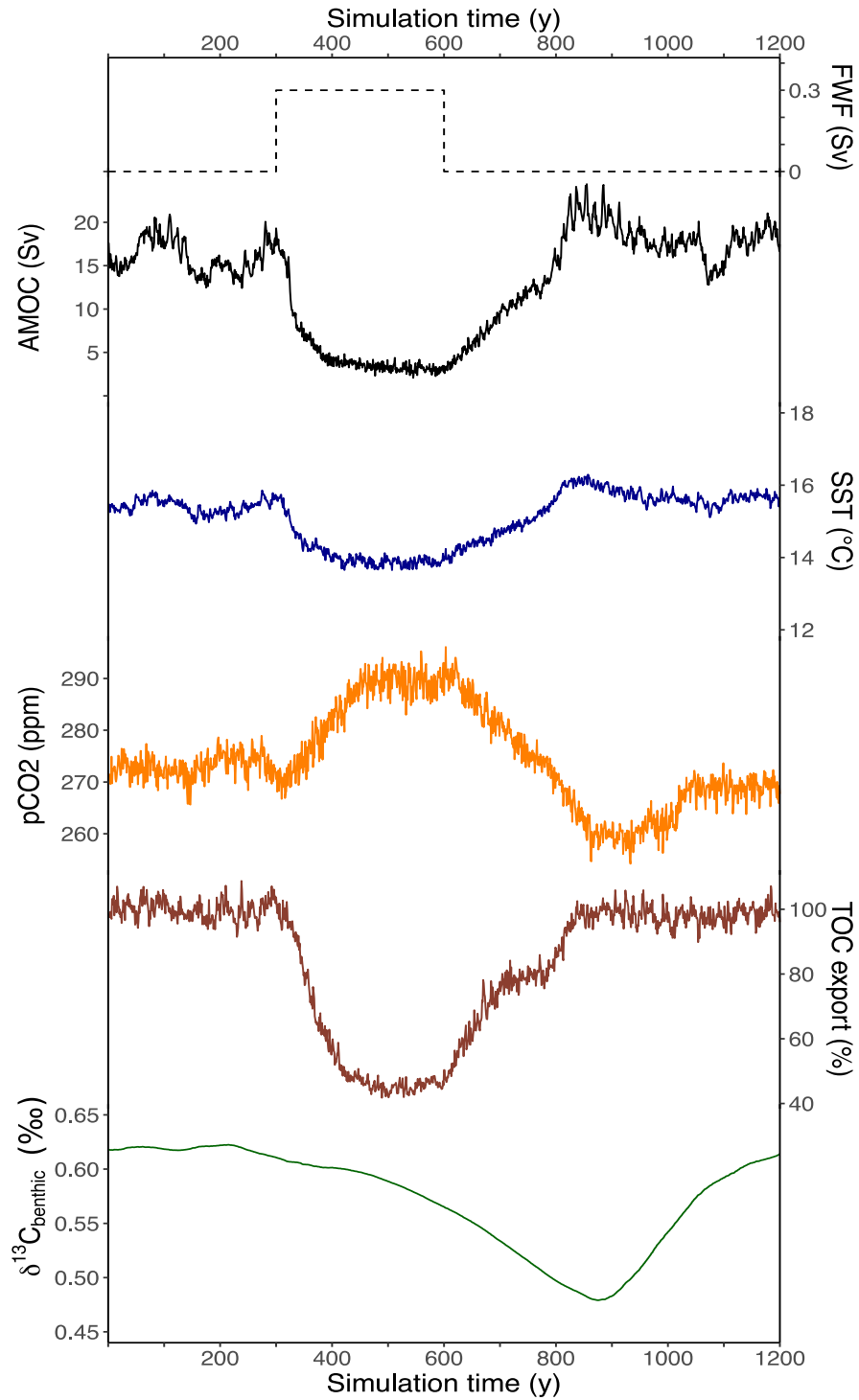
Figure S5: Zonally averaged anomalies for Pa/Th, δ13C and Δ14C in the eastern Atlantic basin in the case of a freshwater input in the Nordic seas.
Same as Figure 3 but for the eastern Atlantic basin.

Figure S6: Zonally averaged response times for Pa/Th, δ13C and Δ14C in the eastern Atlantic basin in the case of a freshwater input in the Nordic seas.
Same as Figure 4 but for the eastern Atlantic basin.

Figure S7: Selected time series during the hosing experiments. From top to bottom: freshwater flux applied to the Nordic Seas (Sv), Maximum of the NADW streamfunction (Sv), the average temperature over the North Atlantic, the aqueous pCO2 (ppm) in the NW Atlantic, the organic carbon export (%) and the δ13C (‰) at the Bermuda Rise (as on Figure 6).
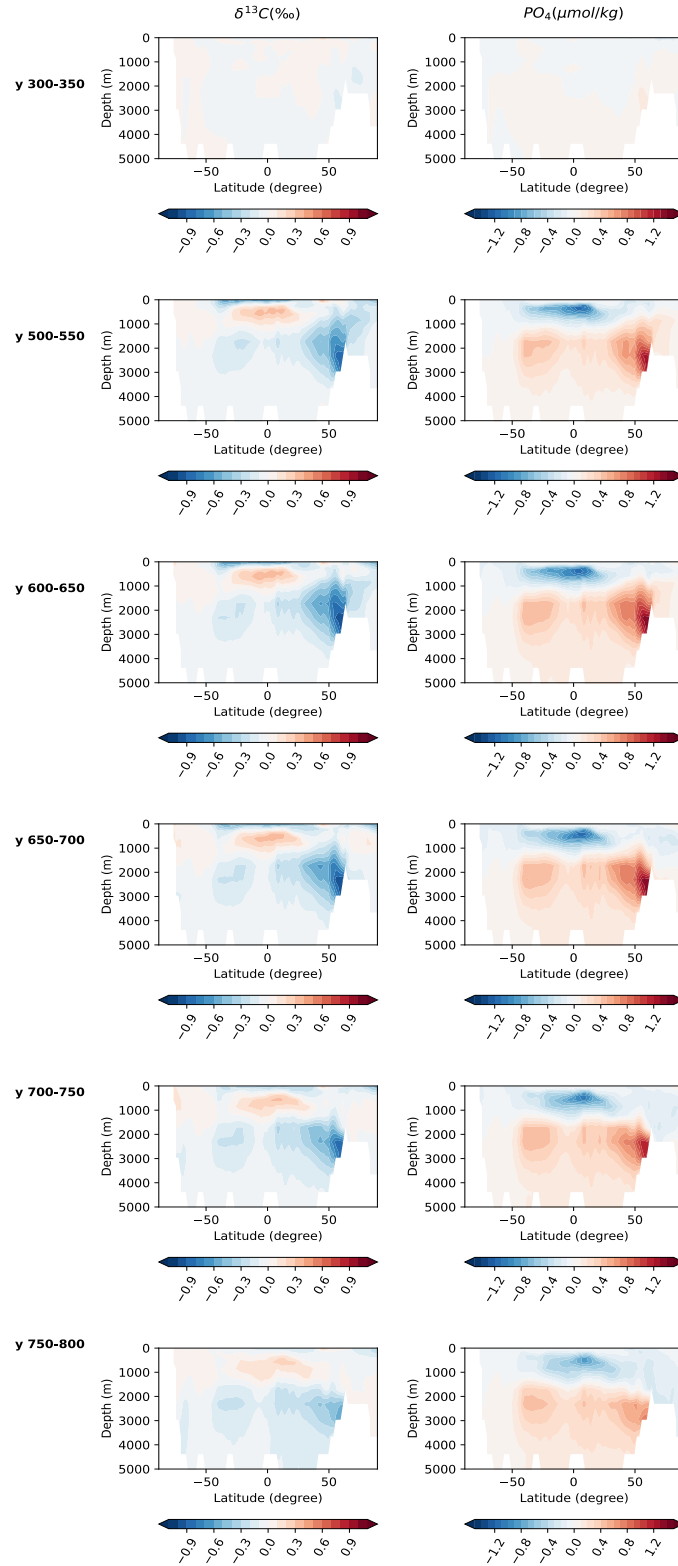
Figure S8: Evolution of the and phosphate anomalies on the Atlantic N-S section. Anomaly denotes the difference between $\delta_{13}C$ (‰) or phosphate (μmol/kg) averaged over the indicated time period (e.g. year 500 to year 550) and the same variable averaged over the control period (i.e. 300 first years of simulation).

References

Chase, Z., Anderson, R. F., Fleisher, M. Q. and Kubik, P. W.: The influence of particle composition and particle flux on scavenging of Th, Pa and Be in the ocean, Earth and Planetary Science Letters, 204(1), 215–229, doi:10.1016/S0012-821X(02)00984-6, 2002.

Deng, F., Thomas, A. L., Rijkenberg, M. J. A. and Henderson, G. M.: Controls on seawater 231Pa, 230Th and 232Th concentrations along the flow paths of deep waters in the Southwest Atlantic, Earth and Planetary Science Letters, 390, 93–102, doi:10.1016/j.epsl.2013.12.038, 2014.

Dutay, J.-C., Lacan, F., Roy-Barman, M. and Bopp, L.: Influence of particle size and type on 231Pa and 230Th simulation with a global coupled biogeochemical-ocean general circulation model: A first approach, Geochemistry, Geophysics, Geosystems, 10(1), 2009.

Gdaniec, S., Roy-Barman, M., Foliot, L., Thil, F., Dapoigny, A., Burckel, P., Garcia-Orellana, J., Masqué, P., Mörth, C.-M. and Andersson, P. S.: Thorium and protactinium isotopes as tracers of marine particle fluxes and deep water circulation in the Mediterranean Sea, Marine Chemistry, 199, 12–23, doi:10.1016/j.marchem.2017.12.002, 2018.

Hayes, C. T., Anderson, R. F., Fleisher, M. Q., Huang, K.-F., Robinson, L. F., Lu, Y., Cheng, H., Edwards, R. L. and Moran, S. B.: 230Th and 231Pa on GEOTRACES GA03, the U.S. GEOTRACES North Atlantic transect, and implications for modern and paleoceanographic chemical fluxes, Deep Sea Research Part II: Topical Studies in Oceanography, 116, 29–41, doi:https://doi.org/10.1016/j.dsr2.2014.07.007, 2015a.

Hayes, C. T., Anderson, R. F., Fleisher, M. Q., Vivancos, S. M., Lam, P. J., Ohnemus, D. C., Huang, K.-F., Robinson, L. F., Lu, Y., Cheng, H., Edwards, R. L. and Moran, S. B.: Intensity of Th and Pa scavenging partitioned by particle chemistry in the North Atlantic Ocean, Marine Chemistry, 170, 49–60, doi:10.1016/j.marchem.2015.01.006, 2015b.

van Hulten, M., Dutay, J.-C. and Roy-Barman, M.: A global scavenging and circulation ocean model of thorium-230 and protactinium-231 with improved particle dynamics (NEMO–ProThorP 0.1), Geosci. Model Dev., 11(9), 3537–3556, doi:10.5194/gmd-11-3537-2018, 2018.

Luo, S. and Ku, T.-L.: On the importance of opal, carbonate, and lithogenic clays in scavenging and fractionating 230Th, 231Pa and 10Be in the ocean, Earth and Planetary Science Letters, 220(1), 201–211, doi:10.1016/S0012-821X(04)00027-5, 2004.

Siddall, M., Henderson, G. M., Edwards, N. R., Frank, M., Müller, S. A., Stocker, T. F. and Joos, F.: 231Pa/230Th fractionation by ocean transport, biogenic particle flux and particle type, Earth and Planetary Science Letters, 237(1), 135–155, doi:10.1016/j.epsl.2005.05.031, 2005.